Journal of Magnetic Resonance 212 (2011) 186–196

Contents lists available at ScienceDirect

Journal of Magnetic Resonance

journal homepage: www.elsevier.com/locate/jmr

Pseudorandom selective excitation in NMR

Jamie D. Walls *, Alexandra Coomes

Department of Chemistry, University of Miami, Coral Gables, FL 33124, USA

ARTICLE INFO

Article history:
Received 4 May 2011
Revised 14 June 2011
Available online 7 July 2011

Keywords:
Selective excitation
Average Hamiltonian theory
DANTE

ABSTRACT

In this work, average Hamiltonian theory is used to study selective excitation under a series of small flip-angle θ-pulses $\left[\theta \ll \frac{\pi}{3}\right]$ applied either periodically [corresponding to the DANTE pulse sequence] or aperiodically to a spin-1/2 system. First, an average Hamiltonian description of the DANTE pulse sequence is developed that is valid for frequencies either at or very far from integer multiples of $\frac{1}{\tau}$, where τ is the interpulse delay. For aperiodic excitation, a single resonance, ν_{sel}, can be selectively excited if the θ-pulse phases are modulated in concert with the interpulse delays. The conditions where average Hamiltonian theory can be accurately applied to describe the dynamics under aperiodic selective pulses, which are referred to as pseudorandom-DANTE or p-DANTE sequences, are similar to those found for the DANTE sequence. Signal averaging over different p-DANTE sequences improves the apparent selectivity at ν_{sel} by reducing the excitations at other frequencies. Experimental demonstrations of p-DANTE sequences and comparisons with the theory are presented.

1. Introduction

Of the multitude of radiofrequency (RF) schemes used for exciting and controlling spin dynamics in NMR, most can be placed into one of two categories: aperiodic RF pulse sequences or periodic RF pulse sequences. For many aperiodic sequences, the RF phases, amplitudes and pulse delays are often chosen randomly or in a pseudorandom manner. Such sequences have been used to generate white noise or broadband excitation in NMR noise spectroscopy [1–4], while sequences that generate colored noise have been used in early spin decoupling schemes, such as in noise decoupling [5]. Theoretical models of a spin system's response to pseudorandom pulse sequences typically use a Volterra or perturbation series in the randomly applied RF pulses [6]. Since many pseudorandom sequences are designed by considering only the first term in the Volterra series, pseudorandom sequences are typically low power and result in small, linear spin excitations.

Unlike aperiodic sequences, periodic RF pulse sequences are commonly used in a variety of NMR experiments and are often found to be superior to their pseudorandom counterparts; for example, two periodic sequences, MLEV [7] and WALTZ-16 [8], provide better heteronuclear decoupling over noise decoupling under most conditions. Many periodic RF pulse sequences are designed using average Hamiltonian theory (AHT) [9], where the necessary RF pulse sequence that generates a desired average Hamiltonian $\overline{H}_{avg}$ over a time τ_c must be determined (τ_c is the length of the pulse sequence). Repeated application of the pulse sequence introduces frequencies into the dynamics that are integer multiples of $\frac{1}{\tau_c}$, which may result in higher-order contributions to $\overline{H}_{avg}$ that degrade the sequence's performance. It has been previously noted that random or asynchronous pulse imperfections placed into pulse sequences can often improve their performance [10]. Recently, Uhrig dynamical decoupling (UDD) sequences [11], which utilize unequally spaced π-pulses, were shown to be superior [12] in preserving spin coherence to the standard Carr–Purcell–Meiboom–Gill (CPMG) sequence [13], which uses equally spaced π-pulses.

Selective pulses [14] are one class of pulses that do not fall neatly into either category. The design of most commonly used selective pulses, such as the gaussian and the sinc pulses, is guided by the fact that the excitation profile of a spin system after an applied RF pulse is proportional to the Fourier transformation of the applied RF pulse [15] within the linear response regime, i.e., for total flip-angle $\Theta \ll \frac{\pi}{3}$. This principle has been used to develop colored noise sequences for selective excitation in imaging applications [16]. While such sequences are valid for small flip-angles, they can fail in the nonlinear regime $\left[\Theta \geqslant \frac{\pi}{3}\right]$. As such, most methods for designing selective pulses of arbitrary flip-angle use the linear response pulse shapes as starting points in numerical searches [17]. However, pulse shapes generated by these numerical techniques often do not lend themselves to an easy physical interpretation behind their selectivity.

One of the earliest and most easily understood periodic selective pulse that is rigorously valid for all flip-angles is the DANTE sequence [18], which is shown in Fig. 1A. The DANTE sequence consists of a series of N small-tip, broadband θ-pulses that selectively rotate only those spins resonating at integer multiples of the interpulse

* Corresponding author.
E-mail address: jwalls@miami.edu (J.D. Walls).

1090-7807/$ - see front matter © 2011 Elsevier Inc. All rights reserved.
doi:10.1016/j.jmr.2011.06.026

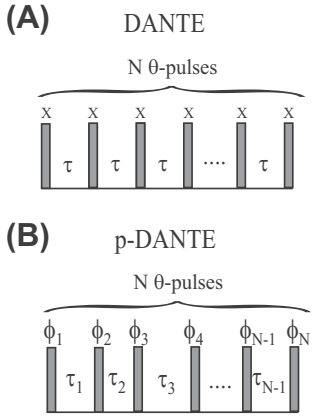

Fig. 1. Pulse sequence for (A) DANTE and (B) pseudorandom-DANTE or p-DANTE selective excitation. (A) The DANTE sequence [18] consists of a series of N small-flip, θ-pulses, equally spaced between periods of free evolution of time τ. The periodicity of the sequence results in a rotation of $\Theta = N\theta$ about an axis perpendicular in the transverse plane for those spins resonating (in the rotating frame) at a frequency $\nu_Z \approx \frac{n}{\tau}$, where n is an integer. (B) The p-DANTE sequence consists of a series of N unequally spaced small-flip, θ-pulses, where τ_k is the time delay between the kth and $(k+1)$th, pulse, and $\phi_k = 2\pi\sum_{k=1}^{k-1}\nu_{sel}\tau_k$ is the phase of the kth pulse with $\phi_1 = 0$. In the p-DANTE sequence, only those spins resonating (in the rotating frame) at $\nu_Z = \nu_{sel}$ are rotated by an angle $\Theta = N\theta$.

delay, $\nu_Z = \frac{n}{\tau}$, by $\Theta = N\theta$ about an axis in the transverse plane. This frequency response results from the periodicity of the θ-pulses, which can be readily seen in the linear response regime [19]. To excite a single frequency, however, the periodicity of the DANTE sequence must be violated. Breaking DANTE's symmetry in order to reduce excitation at other frequencies has been previously accomplished by modulating the phases [20], amplitudes, and delays of the θ-pulses [21]. However, most modifications of the DANTE sequence that result in exciting only a single frequency are still based on the assumption of linear response, $\Theta \ll \frac{\pi}{3}$.

In this work, AHT is applied to describe the selective excitation in NMR by pseudorandom-DANTE sequences (Fig. 1B), which are a class of experiments consisting of a series of small, flip-angle pulses, where the interpulse delays and phases are modulated. The outline for this paper is as follows: first, the conditions, where AHT can be applied to the DANTE pulse sequence are determined. Because AHT is often used as a guiding principle in pulse sequence design, understanding the limits of AHT's application to aperiodic sequences is useful since there are no general theories to handle aperiodic, nonlinear excitation (except by direct numerical simulation). Next, an AHT description for a series of aperiodically spaced and phase-modulated θ-pulses is developed. Such sequences are referred to as pseudorandom-DANTE or p-DANTE selective pulses [Fig. 1(B)]. Finally, experiments performed in acetone and in an acetone/DMSO/water solution are used to demonstrate and validate the selectivity of the p-DANTE sequences along with the theoretical results presented in this work.

2. General theory

Both the DANTE (Fig. 1A) and the p-DANTE (Fig. 1B) pulse sequences involve the application of a series of N small flip-angle θ-pulses that selectively rotate spins about an axis lying in the transverse plane by an angle $\Theta = N\theta$. For the DANTE sequence, spins resonating at $\nu_Z = \frac{n}{\tau}$ are selectively rotated by Θ (where n is an integer), whereas for the p-DANTE sequence, only those spins resonating at $\nu_Z = \nu_{sel}$ are rotated by Θ. To understand the selectivity of both the DANTE and p-DANTE sequences within the framework of AHT, it is useful to revisit the dynamics of a spin-1/2 system under nonresonant RF irradiation. The Hamiltonian during the application of an RF pulse is given by $\frac{\widehat{H}}{\hbar} = \omega_z\widehat{I}_Z + \omega_{RF}(\widehat{I}_X\cos(\phi) + \widehat{I}_Y\sin(\phi))$, where ϕ and ω_{RF} are the phase and amplitude of the RF pulse, $\omega_Z = 2\pi\nu_Z$ is the resonance offset that the spin experiences in the rotating frame, and $\widehat{I}_j = \frac{1}{2}\widehat{\sigma}_j$ for $j = \{X,Y,Z\}$ are spin-1/2 operators with $\widehat{\boldsymbol{\sigma}}$ being the Pauli spin matrices.

The propagator for an RF pulse applied for a time T_p can be written as:

$$\begin{aligned}\widehat{P}_\phi^{\text{exact}}(T_p) &= \exp\left(-\frac{i}{\hbar}\widehat{H}T_p\right)\\ &= \exp\left(-i\left[\omega_Z\widehat{I}_Z + \omega_{RF}\left(\widehat{I}_X\cos(\phi) + \widehat{I}_Y\sin(\phi)\right)\right]T_p\right)\\ &= \cos(\omega_{\text{EFF}}T_p)\widehat{1} - i\sin(\omega_{\text{EFF}}T_p)\\ &\quad\left(\frac{\omega_Z}{\omega_{\text{EFF}}}\widehat{I}_Z + \frac{\omega_{RF}}{\omega_{\text{EFF}}}(\cos(\phi)\widehat{I}_X + \sin(\phi)\widehat{I}_Y)\right)\end{aligned} \tag{1}$$

where $\omega_{\text{EFF}} = \frac{\sqrt{\omega_Z^2+\omega_{RF}^2}}{2}$ and $\hat{1}$ is the two-dimensional identity operator.

Alternatively, the propagator in Eq. (1) can be transformed into an interaction frame defined by $\widehat{U}_{\text{free}}(\omega_Z t) = \exp(-i\omega_Z t\widehat{I}_Z)$ and can be written as:

$$\begin{aligned}\widehat{P}_\phi^{\text{exact}}(T_p) &= \widehat{U}_{\text{free}}(\omega_Z T_p)\widehat{T}\exp\left(-i\int_0^{T_p}\frac{\omega_{RF}}{2}\left[\widehat{I}_+e^{i(\omega_Z t'-\phi)}\right.\right.\\ &\quad\left.\left.+\widehat{I}_-e^{-i(\omega_Z t'-\phi)}\right]dt'\right)\\ &= \widehat{U}_{\text{free}}(\omega_Z T_p)\widehat{T}\exp\left(-\frac{i}{\hbar}\int_0^{T_p}\widehat{H}_{INT,\phi}(t')dt'\right)\end{aligned} \tag{2}$$

where $\widehat{T}$ is the Dyson time-ordering operator [22], and $\widehat{H}_{INT,\phi}(t) = \frac{\omega_{RF}}{2}\left(\widehat{I}_+e^{i(\omega_Z t-\phi)} + \widehat{I}_-e^{-i(\omega_Z t-\phi)}\right)$, is the Hamiltonian in the interaction frame, which in this case represents a purely phase-modulated RF pulse. Using AHT [9,23], the time-dependent propagator in Eq. (2) can be approximated by:

$$\widehat{T}\exp\left(-\frac{i}{\hbar}\int_0^{T_p}\widehat{H}_{INT,\phi}(t')dt'\right) = \exp\left(-\frac{i}{\hbar}\overline{H}_{p,\phi}T_p\right) \tag{3}$$

In Eq. (3), $\overline{H}_{p,\phi} = \sum_{n=1}^{\infty}\overline{H}_{p,\phi}^{(n)}$ is the average Hamiltonian, where the first two terms in the series are:

$$\begin{aligned}\frac{\overline{H}_{p,\phi}^{(1)}}{\hbar} &= \frac{1}{\hbar T_p}\int_0^{T_p}\widehat{H}_{INT,\phi}(t')dt'\\ &= \frac{\omega_{RF}}{2}\text{sinc}\left(\frac{\omega_Z T_p}{2}\right)\left(\widehat{I}_+e^{i\left(\frac{\omega_Z T_p}{2}-\phi\right)} + \widehat{I}_-e^{-i\left(\frac{\omega_Z T_p}{2}-\phi\right)}\right)\\ \frac{\overline{H}_{p,\phi}^{(2)}}{\hbar} &= \frac{1}{2iT_p\hbar^2}\int_0^{T_p}\int_0^{t'}\left[\widehat{H}_{INT,\phi}(t'),\widehat{H}_{INT,\phi}(t'')\right]dt'dt''\\ &= \frac{\omega_{RF}^2}{4iT_p}\widehat{I}_Z\int_0^{T_p}dt'\int_0^{t'}dt''\left(e^{i\omega_Z(t'-t'')} - e^{-i\omega_Z(t'-t'')}\right)\\ &= \frac{\omega_{RF}^2}{2\omega_Z}[1-\text{sinc}(\omega_Z T_p)]\widehat{I}_Z\end{aligned} \tag{4}$$

$\widehat{P}_\phi^{\text{exact}}(T_p)$ in Eq. (2) can be approximated as:

$$\widehat{P}_\phi^{\text{exact}}(T_p) \approx \widehat{P}_\phi(T_p) \approx \widehat{U}_{\text{free}}(\omega_Z T_p)\exp\left(-\frac{i}{\hbar}\left(\overline{H}_{p,\phi}^{(1)} + \overline{H}_{p,\phi}^{(2)}\right)T_p\right) \tag{5}$$

For $\omega_{RF}T_p \leqslant \frac{2\pi}{9}$, $\left\|\widehat{P}_\phi^{\text{exact}}(T_p) - \widehat{P}_\phi(T_p)\right\| \leqslant 10^{-3}$ for all ω_Z, where $\|A\| = \sqrt{\text{Tr}[A^\dagger A]}$ represents the Frobenius matrix norm. For instance, if A and B are two $n\times n$ unitary matrices, then $\|A-B\|$ represents a measure of the "length/distance" between A and B, with the maximum value of $\|A-B\|$being $2\sqrt{n}$. Since the DANTE and p-DANTE sequences both consist of a series of small flip-angle θ-pulses with

$\theta < \frac{2\pi}{9}$, the approximation $\hat{P}_{\phi}^{\text{exact}}(T_p) \approx \hat{P}_{\phi}(T_p)$ in Eq. (5) will be used in the rest of this paper.

For future comparison of the propagator in Eq. (2) with the propagator under either the DANTE or the p-DANTE sequences in Fig. 1, it is useful to consider an alternative description of $\hat{P}_{\phi}^{\text{exact}}(T_p)$ in the interaction frame by dividing $\hat{T}\exp\left(-\frac{i}{\hbar}\int_0^{T_p}\hat{H}_{INT,\phi}(t')dt'\right)$ in Eq. (2) into $N \gg 1$ smaller propagators of duration $\Delta T = \frac{T_p}{N}$, which is illustrated in Fig. 2A. In this case, $P_{\phi}^{\text{exact}}(T_p)$ can be rewritten as:

$$\begin{aligned}\hat{P}_{\phi}^{\text{exact}}(T_p) &= \hat{U}_{\text{free}}(\omega_Z T_p)\hat{T}\exp\left(-\frac{i}{\hbar}\int_0^{T_p}\hat{H}_{INT,\phi}(t')dt'\right)\\ &= \hat{U}_{\text{free}}(\omega_Z T_p)\hat{T}\prod_{j=0}^{N-1}\exp\left(-\frac{i}{\hbar}\int_{j\Delta T}^{(j+1)\Delta T}\hat{H}_{INT,\phi}(t')dt'\right)\\ &\approx \hat{U}_{\text{free}}(\omega_Z T_p)\hat{T}\prod_{j=0}^{N-1}\exp\left(-i\omega_{RF}\Delta T\,\text{sinc}\left(\frac{\omega_Z\Delta T}{2}\right)\right.\\ &\quad\left.\left(\hat{I}_X\cos\left(\phi_j^*\right)-I_Y\sin\left(\phi_j^*\right)\right)\right)\end{aligned} \tag{6}$$

where $\phi_j^* = \left(j+\frac{1}{2}\right)\omega_Z\Delta T - \phi$. With respect to Eq. (6) and Fig. 2A, the total propagator for an RF pulse of strength ω_{RF} applied off-resonantly by ω_Z for a time T_p is equivalent to the application of a series of N small-flip, phase-modulated RF pulses followed by a rotation about the $\hat{z}$-axis by $\omega_Z T_p$, where the flip angle and phase of the $(j+1)$th pulse are $\theta = \omega_{RF}\Delta T\,\text{sinc}\left(\frac{\omega_Z\Delta T}{2}\right)$ and $-\phi_j^*$ respectively.

2.1. DANTE pulse sequence

In this section, we present an AHT description of the DANTE pulse sequence (Fig. 1A) that is valid outside the linear response regime $\left[\Theta > \frac{\pi}{3}\right]$. While an analytical expression for DANTE is known when the θ-pulses are applied on resonance [24], there currently does not exist a quantitative analytical theory for the effective excitation under p-DANTE sequences (Fig. 1B) when aperiodic delays, pulse angles, and/or nonconstant flip angles are used. Understanding the limits of AHT applied to the DANTE sequence can therefore help to determine the conditions where an AHT description of the p-DANTE sequences are also valid.

As mentioned in the introduction, the DANTE sequence [18] consists of a series of N, equally spaced small-tip, θ-pulses of constant phase and duration t_p, where $\omega_{RF}t_p = \theta \ll \frac{\pi}{3}$ (Fig. 1A). The full propagator for the DANTE pulse sequence can be written as [for $\phi = 0$]:

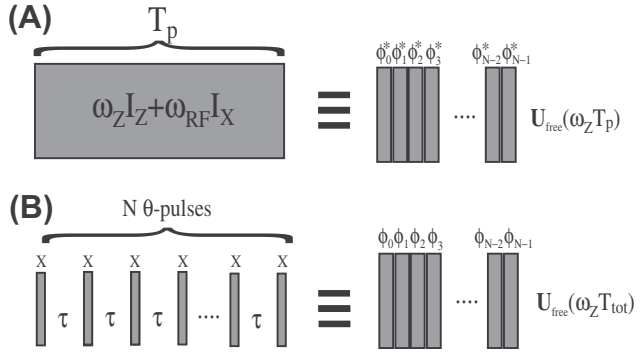

Fig. 2. The connection between the DANTE pulse sequence and the application of an off-resonant RF pulse. (A) An RF pulse of strength ω_{RF} applied off resonance by ω_Z for a time T_p is equivalent to applying $N \gg 1$ phase-modulated, small flip-angle $\theta = \frac{\omega_{RF}T_p}{N}\,\text{sinc}\left(\frac{\omega_Z T_p}{2N}\right)$ pulses followed by a rotation about the $\hat{z}$-axis by an angle $\omega_Z T_p$. The phase of the $(k+1)$th pulse is given by $\phi_k^* = -\left(k+\frac{1}{2}\right)\frac{\omega_Z T_p}{N} + \phi$ [in 2A, $\phi = 0$]. (B) The DANTE pulse sequence is equivalent to a series of N phase-modulated small-flip pulses followed by a rotation about the $\hat{z}$-axis by an angle $N\omega_Z\tau$ [Eq. (7)]. The phase of the $(k+1)$th pulse is $\phi_k = -\omega_Z\left(k\tau_t + \frac{t_p}{2}\right)$, where $\tau_t = \tau + t_p$, t_p is the length of the small-flip pulses, and $T_{\text{tot}} = (N-1)\tau_t + t_p$.

$$\begin{aligned}\hat{U}_{\text{exact}}(T_{\text{tot}}) &= \hat{P}_0(t_p)(\hat{U}_{\text{free}}(\omega_Z\tau)\hat{P}_0(t_p))^{N-1}\\ &= (\hat{P}_0(t_p)\hat{U}_{\text{free}}(\omega_Z\tau))^{N-1}\hat{P}_0(t_p)\\ &= \hat{U}_{\text{free}}(\omega_Z T_{\text{tot}})\hat{T}\prod_{k=0}^{N-1}\hat{P}_{-k\omega_Z\tau_t}(t_p)\end{aligned} \tag{7}$$

where τ is the time delay between pulses, $\tau_t = \tau + t_p$, $T_{\text{tot}} = (N-1)\tau_t + t_p$, and

$$\begin{aligned}\hat{P}_{-k\omega_Z\tau_t}(t_p) &= \hat{U}_{\text{free}}^{\dagger}(k\omega_Z\tau_t)\hat{P}_0(t_p)\hat{U}_{\text{free}}(k\omega_Z\tau_t)\\ &\equiv \exp\left(-\frac{i}{\hbar}\hat{H}_k t_p\right)\end{aligned} \tag{8}$$

where $\hat{H}_k$ is given by [using Eq. (4)]:

$$\begin{aligned}\frac{\hat{H}_k}{\hbar} &\approx \hat{U}_{\text{free}}^{\dagger}(k\omega_Z\tau_t)\left(\frac{\overline{H}_{p,0}^{(1)}+\overline{H}_{p,0}^{(2)}}{\hbar}\right)\hat{U}_{\text{free}}(k\omega_Z\tau_t)\\ &= \frac{\overline{H}_{p,-k\omega_Z\tau_t}^{(1)}+\overline{H}_{p,-k\omega_Z\tau_t}^{(2)}}{\hbar}\\ &= \frac{\omega_{RF}}{2}\,\text{sinc}\left(\frac{\omega_Z t_p}{2}\right)\left(\hat{I}_+ e^{i\omega_Z\left(k\tau_t+\frac{t_p}{2}\right)}+\hat{I}_- e^{-i\omega_Z\left(k\tau_t+\frac{t_p}{2}\right)}\right)\\ &+\frac{\omega_{RF}^2}{2\omega_Z}(1-\text{sinc}(\omega_Z t_p))\hat{I}_Z\\ &= \frac{a}{2}\left(\hat{I}_+ e^{i\omega_Z\left(k\tau_t+\frac{t_p}{2}\right)}+\hat{I}_- e^{-i\omega_Z\left(k\tau_t+\frac{t_p}{2}\right)}\right)+b\hat{I}_Z\end{aligned} \tag{9}$$

where $a = \omega_{RF}\,\text{sinc}\left(\frac{\omega_Z t_p}{2}\right)$ and $b = \frac{\omega_{RF}^2}{2\omega_Z}(1-\text{sinc}(\omega_Z t_p))$. As has been previously noted [25–27], the propagator for the DANTE sequence in Eq. (7) is the same as the propagator for a continuous series of N, phase modulated small-flip pulses, where the phase modulation depends upon the spin's resonance offset, $\omega_Z = 2\pi\nu_Z$, followed by an overall rotation about the $\hat{z}$-axis by $\omega_Z T_{\text{tot}}$. This is illustrated in Fig. 2B. If $\text{mod}[\omega_Z\tau_t, 2\pi] \approx 0$ (where $\text{mod}[a,b]$ gives the positive remainder of a/b), then all N pulses are effectively applied along the same direction since $\phi_k \approx \phi_j$ for all k and j. The small θ pulses are therefore additive and result in an overall rotation of $\Theta \approx N\theta$ about an axis in the transverse plane. When $\text{mod}[\omega_Z\tau_t, 2\pi] \neq 0$, the θ-pulses are applied about different directions [$\phi_k \neq \phi_j$ for $k \neq j$ in general] thereby reducing the overall spin nutation. Comparing Fig. 2B and Eqs. (7) and (9) with Fig. 2A and Eq. (6), the propagator for the DANTE sequence is similar to the propagator for an off-resonant, RF pulse of duration $T_p = Nt_p$ followed by a rotation about the $\hat{z}$-axis. That is, Eq. (7) can be written as:

$$\begin{aligned}\hat{U}_{\text{exact}}(T_{\text{tot}}) \approx &\hat{U}_{\text{free}}(\omega_Z T_{\text{tot}} - \omega_Z' T_p)\\ &\exp[-iT_p\left(\omega_Z'\hat{I}_Z + \omega_{RF}'\left(\hat{I}_X\cos(\phi') + \hat{I}_Y\sin(\phi')\right)\right)]\end{aligned} \tag{10}$$

where $\omega_Z' = \frac{2\pi}{t_p}\text{mod}[\omega_Z\tau_t, 2\pi]$, $\omega_{RF}' = \frac{\text{sinc}\left(\frac{\omega_Z t_p}{2}\right)}{\text{sinc}\left(\frac{\omega_Z' t_p}{2}\right)}\omega_{RF}$, and $\phi' = (\omega_Z' - \omega_Z)\frac{t_p}{2}$.

As mentioned above, when $\text{mod}[\omega_Z\tau_t, 2\pi] = 0$, $\omega_Z' = 0$, and the pulses are effectively applied on resonance, maximally rotating the spin by Θ. When $\text{mod}[\omega_Z\tau_t, 2\pi] \neq 0$, then ω_Z' can be quite large since $\frac{2\pi}{t_p} \gg 1$ for short pulses ($t_p \ll 1$). When $\omega_Z' \gg \omega_{RF}'$, the effective pulse appears to be applied very far from resonance, resulting in negligible spin excitation.

We now consider using AHT to describe the DANTE pulse sequence and to determine under what conditions an AHT description of DANTE are valid. In the AHT description, the total propagator can be approximated by $\hat{U}(T_{\text{tot}}) \approx \hat{U}_{\text{AHT}}(T_{\text{tot}})$ in Eq. (7), where $\hat{U}_{\text{AHT}}(T_{\text{tot}}) = \hat{U}_{\text{free}}(\omega_Z T_{\text{tot}})\exp\left(-\frac{i}{\hbar}\overline{H}_{\text{avg}}Nt_p\right)$ and $\overline{H}_{\text{avg}} = \sum_{n=1}^{\infty}\overline{H}_{\text{avg}}^{(n)}$ is the average Hamiltonian. The first term in $\overline{H}_{\text{AHT}}$ is given by [using Eq. (A1)]:

$$\begin{aligned}\frac{\overline{H}^{(1)}_{\text{avg}}}{\hbar} &= \frac{1}{Nt_p\hbar}\sum_{k=0}^{N-1}\widehat{H}_k t_p \\ &= \frac{1}{N}\left(\sum_{k=0}^{N-1}\frac{a}{2}\left[\widehat{I}_+ e^{i\omega_Z\left(k\tau_t+\frac{t_p}{2}\right)} + \widehat{I}_- e^{-i\omega_Z\left(k\tau_t+\frac{t_p}{2}\right)}\right] + b\widehat{I}_Z\right) \\ &= b\widehat{I}_Z + \frac{a}{2}\frac{\sin\left(\frac{N\omega_Z\tau_t}{2}\right)}{N\sin\left(\frac{\omega_Z\tau_t}{2}\right)}\left(e^{i\frac{\omega_Z T_{\text{tot}}}{2}}\widehat{I}_+ + e^{-i\frac{\omega_Z T_{\text{tot}}}{2}}\widehat{I}_-\right) \\ &= a\frac{\text{sinc}\left(\frac{N\omega_Z\tau_t}{2}\right)}{\text{sinc}\left(\frac{\omega_Z\tau_t}{2}\right)}\widehat{I}_T(\omega_Z,\tau_t,t_p,N) + b\widehat{I}_Z \end{aligned} \quad (11)$$

where $\widehat{I}_T(\omega_Z,\tau_t,t_p,N) = \widehat{I}_X\cos\left(\frac{\omega_Z T_{\text{tot}}}{2}\right) - \widehat{I}_Y\sin\left(\frac{\omega_Z T_{\text{tot}}}{2}\right)$.

Using Eqs. (A3) and (A4), the second term in $\overline{H}_{\text{avg}}, \overline{H}^{(2)}_{\text{avg}}$, is given by:

$$\begin{aligned}\frac{\overline{H}^{(2)}_{\text{avg}}}{\hbar} &= \frac{1}{2iNt_p\hbar^2}\sum_{k>j}[\widehat{H}_k t_p, \widehat{H}_j t_p] \\ &= \frac{t_p}{2iN}\sum_{k>j}\left[\frac{a}{2}\left(e^{i\omega_Z\left(k\tau_t+\frac{t_p}{2}\right)}\widehat{I}_+ + e^{-i\omega_Z\left(k\tau_t+\frac{t_p}{2}\right)}\widehat{I}_-\right)\right. \\ &\left. + b\widehat{I}_Z, \frac{a}{2}\left(e^{i\omega_Z\left(j\tau_t+\frac{t_p}{2}\right)}\widehat{I}_+ + e^{-i\omega_Z\left(j\tau_t+\frac{t_p}{2}\right)}\widehat{I}_-\right) + b\widehat{I}_Z\right] \\ &= \frac{t_p ab}{4iN}\sum_{k>j}\left(e^{i\omega_Z\left(j\tau_t+\frac{t_p}{2}\right)} - e^{-i\omega_Z\left(k\tau_t+\frac{t_p}{2}\right)}\right)\widehat{I}_+ \\ &\quad - \left(e^{-i\omega_Z\left(j\tau_t+\frac{t_p}{2}\right)} - e^{-i\omega_Z\left(k\tau_t+\frac{t_p}{2}\right)}\right)\widehat{I}_- \\ &\quad + \frac{a^2 t_p}{4iN}\widehat{I}_Z\sum_{k>j}e^{i\omega_Z(k-j)\tau_t} - e^{-i\omega_Z(k-j)\tau_t} \\ &= -\frac{a^2 t_p}{2\omega_Z\tau_t}\frac{\text{sinc}(N\omega_Z\tau_t) - \text{sinc}(\omega_Z\tau_t)}{\left(\text{sinc}\left(\frac{\omega_Z\tau_t}{2}\right)\right)^2}\widehat{I}_Z \\ &\quad + \frac{abt_p(N^2-1)}{2N\omega_Z\tau_t}\frac{\text{sinc}\left(\frac{(N+1)\omega_Z\tau_t}{2}\right) - \text{sinc}\left(\frac{(N-1)\omega_Z\tau_t}{2}\right)}{\text{sinc}^2\left(\frac{\omega_Z\tau_t}{2}\right)} \\ &\quad \times \widehat{I}_T(\omega_Z,\tau_t,t_p,N) \end{aligned} \quad (12)$$

Although the form of $\overline{H}_{\text{avg}}$ for the DANTE sequence is somewhat complicated, the physical picture behind $\overline{H}_{\text{avg}}$ in Eqs. (11) and (12) can be seen in Fig. 2B. When $\omega_Z\tau_t = 2\pi n$ for integer n, $[\widehat{H}_k, \widehat{H}_j] = 0$ for all k and j since $\phi_k = \phi_j$, so $\overline{H}_{\text{avg}} = \overline{H}^{(1)}_{\text{avg}}$ exactly. In this case, the propagator represents a rotation about an axis in the transverse plane of phase $-[(N-1)n\pi + \omega_Z t_p/2]$ by a total angle of $\Theta = N\omega_{RF}t_p\,\text{sinc}(\omega_Z t_p/2) \approx N\omega_{RF}t_p = N\theta$ for $\omega_Z t_p \ll 1$. For $\omega_Z\tau_t \neq 2\pi n$ for integer n, the various $\widehat{H}_k$ are pointing in different directions, which results in a reduction to the average transverse field in $\overline{H}^{(1)}_{\text{avg}}$. Furthermore, since the effective rotation directions no longer commute with one another, that is, $[\widehat{H}_k, \widehat{H}_j] \neq 0$ for $k \neq j$, there is a contribution to $\overline{H}_{\text{avg}}$ at second-order, $\overline{H}^{(2)}_{\text{avg}}$, of an effective field along the $\hat{z}$ direction. When $\left|\overline{H}^{(2)}_{\text{avg}}\right| \gg \left|\overline{H}^{(1)}_{\text{avg}}\right|$, the effective field lies mostly about the $\hat{z}$-axis and the spins are minimally excited (this argument is similar to the concept of second-averaging [28]).

In order to see under what conditions AHT can accurately describe the DANTE pulse sequence, Fig. 3 shows $\|\widehat{U}_{\text{exact}}(T_{\text{tot}}) - \widehat{U}_{\text{AHT}}(T_{\text{tot}})\|$ using $\overline{H}_{\text{avg}} \approx \overline{H}^{(1)}_{\text{avg}} + \overline{H}^{(2)}_{\text{avg}}$, as a function of N and ω_Z/ω_{RF}. Two calculations are shown in Fig. 3, one for a total pulse rotation of $\Theta = \pi/2$ (Fig. 3A) and one for $\Theta = 2\pi$ (Fig. 3B). In both calculations, $\frac{\tau}{t_p} = 1000$. As mentioned above, $\widehat{U}_{\text{AHT}}(T_{\text{tot}}) \approx \widehat{U}_{\text{exact}}(T_{\text{tot}})$ when $2\pi n = \omega_Z\tau_t = \frac{\omega_Z}{\omega_{RF}}\omega_{RF}t_p\left(\frac{\tau}{t_p}+1\right) = \frac{\omega_Z}{\omega_{RF}}\frac{\Theta}{N}\left(\frac{\tau}{t_p}+1\right)$, where n is an integer. Therefore, at a resonance condition for $n \neq 0$, there exists a linear relationship between N and $\frac{\omega_Z}{\omega_{RF}}$ that is given by

$$N = \text{INT}\left[\frac{\omega_Z}{\omega_{RF}}\frac{\Theta}{2\pi n}\left(\frac{\tau}{t_p}+1\right)\right] \quad (13)$$

where INT[x] gives the nearest integer to x. From Fig. 3, for $\theta \leqslant \frac{\pi}{60}$ ($N \geqslant 30$ in Fig. 3A and $N \geqslant 120$ in Fig. 3B), $\widehat{U}_{\text{AHT}}(T_{\text{tot}})$ is a good approximation to $\widehat{U}_{\text{exact}}(T_{\text{tot}})$ for all $\frac{\omega_Z}{\omega_{RF}}$ except near the resonance conditions in Eq. (13). The deviations of $\widehat{U}_{\text{AHT}}(T_{\text{tot}})$ from $\widehat{U}_{\text{exact}}(T_{\text{tot}})$ occur when ω_Z is slightly above or below the DANTE resonance conditions, $\omega_Z = \frac{2\pi n}{\tau_t}$ for integer n. From numerical calculations, the range of frequencies in which $\widehat{U}_{\text{AHT}}(T_{\text{tot}})$ is a good approximation to $\widehat{U}_{\text{exact}}(T_{\text{tot}})$ was found to be given by $\delta\omega_Z \gg \frac{6\theta\pi}{5\tau_t\Theta}$ or $\delta\omega_Z \ll \frac{6\theta\pi}{5\tau_t\Theta}$, where $\delta\omega_Z = \min\left[\left|\,\omega_Z - \frac{2\pi n}{\tau_t}\,\right|\right]$ is the smallest frequency difference between ω_Z and the nearest integer multiple of the DANTE resonance frequency, $\frac{2\pi}{\tau_t}$. This can be seen in the inset shown in Fig. 3A, where $\|\widehat{U}_{\text{AHT}}(T_{\text{tot}}) - \widehat{U}_{\text{exact}}(T_{\text{tot}})\|$ is largest just above and below the resonance condition given by Eq. (13). Although the range of ω_Z, where $\widehat{U}_{\text{AHT}}(T_{\text{tot}})$ is a good approximation increases with

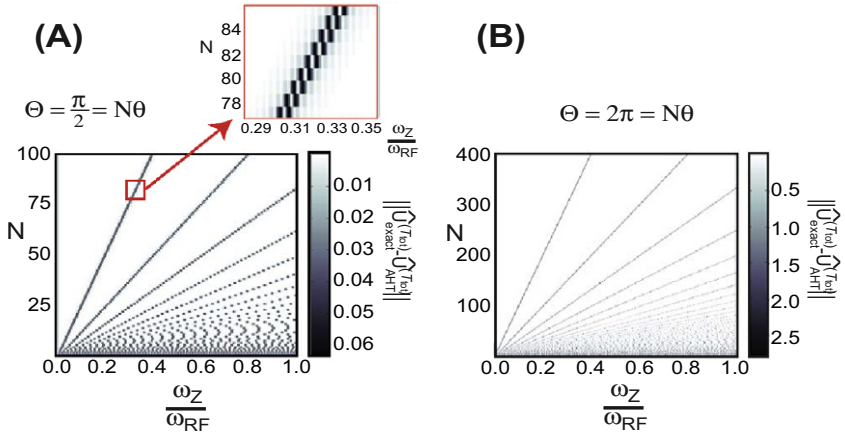

Fig. 3. (Color online) The Frobenius norm of $\|\widehat{U}_{\text{exact}}(T_{\text{tot}}) - \widehat{U}_{\text{AHT}}(T_{\text{tot}})\|$ as a function of the number of small tip θ-pulses, N, and the ratio of the resonance offset to the applied RF, $\frac{\omega_Z}{\omega_{RF}}$. In this figure, two calculations are shown for total maximum flip angle of (A) $\Theta = \frac{\pi}{2}$ and (B) $\Theta = 2\pi$. $\widehat{U}_{\text{exact}}(T_{\text{tot}})$ [Eq. (7)] is the exact propagator for the DANTE sequence, and $\widehat{U}_{\text{AHT}}(T_{\text{tot}})$ is the propagator calculated using the average Hamiltonian, $\overline{H}_{\text{avg}} \approx \overline{H}^{(1)}_{\text{avg}} + \overline{H}^{(2)}_{\text{avg}}$ in Eqs. (11) and (12). In both calculations, $\frac{\tau}{t_p} = 1000$. The greatest deviations between $\widehat{U}_{\text{exact}}(T_{\text{tot}})$ and $\widehat{U}_{\text{AHT}}(T_{\text{tot}})$ occur slightly above and below the resonance conditions in Eq. (13) with the maxima in $\|\widehat{U}_{\text{exact}}(T_{\text{tot}}) - \widehat{U}_{\text{AHT}}(T_{\text{tot}})\|$ approximately described by two parallel lines given by $N = \text{INT}\left[\frac{\omega_Z}{\omega_{RF}}\frac{\Theta}{2\pi n}\left(\frac{\tau}{t_p}+1\right) \pm \frac{3}{5n}\right]$ for integer $n \neq 0$. This is more clearly shown in the inset of 3A. The agreement between $\widehat{U}_{\text{AHT}}(T_{\text{tot}})$ and $\widehat{U}_{\text{exact}}(T_{\text{tot}})$ also improves with decreasing Θ.

decreasing θ (increasing N), the maximum of $\|\hat{U}_{\mathrm{AHT}}(T_{tot}) - \hat{U}_{\mathrm{exact}}(T_{tot})\|$ mainly depends upon the overall rotation angle, Θ. For $\Theta \leqslant \frac{5\pi}{9}$, $\max[\|\hat{U}_{\mathrm{AHT}}(T_{tot}) - \hat{U}_{\mathrm{exact}}(T_{tot})\|] \leqslant 0.1$ for all N and ω_Z. For $\Theta = 2\pi$ in Fig. 3B, the propagator using up to the second-order AHT breaks down for ω_Z slightly above and below the DANTE resonance conditions, where $\max[\|\hat{U}_{\mathrm{AHT}}(T_{tot}) - \hat{U}_{\mathrm{exact}}(T_{tot})\|] = 2.81 \approx 2\sqrt{2}$. This is consistent with earlier results [29] that the convergence of the Magnus expansion for the average Hamiltonian breaks down for rotations greater or equal to 2π. Physically, this can be understood as follows: for $\delta\omega_Z \gg \frac{6\theta\pi}{5\tau_t\Theta}$, the effective phases of the pulses (see Fig. 2B) are modulated faster than the strength of the RF, that is, $\delta\omega_Z \gg \omega_{RF}$. In this case, the small-tip pulses effectively average to zero, leading to negligible spin nutation. For $\delta\omega_Z \ll \frac{6\pi\theta}{5\tau_t\Theta}$, the phases of the pulses in Fig. 2B are relatively unchanged during the course of the sequence; in this case, the various Hamiltonians, $\hat{H}_k$ in Eq. (9), commute with one another, so $\overline{H}_{\mathrm{avg}} \approx \overline{H}^{(1)}_{\mathrm{avg}}$ and $\hat{U}_{\mathrm{exact}}(T_{tot}) \approx \hat{U}_{\mathrm{AHT}}(T_{tot})$. In the intermediate range, where $\delta\omega_Z \sim \frac{6\pi\theta}{5\tau_t\Theta}$, the phase modulation is comparable to the strength of the RF, and there exists no "small" parameter to utilize in the expansion of the average Hamiltonian (i.e., higher-order terms greater than second-order must be considered and/or exact calculation of the propagator must be performed).

2.2. pseudorandom DANTE (p-DANTE)

In the DANTE sequence, a natural frequency of $\frac{1}{\tau_t}$ is introduced into the dynamics, resulting in efficient excitation at frequencies $\nu_Z = \frac{n}{\tau_t}$ for integer n. However, suppose that one was interested in using a DANTE-like sequence to efficiently excite only one particular frequency, say at $\nu_Z = 0$ Hz. One way to accomplish this using a DANTE sequence would be to make τ_t small enough such that all DANTE frequencies, $\frac{n}{\tau_t}$ for $n \neq 0$, lie outside the relevant spectral width. If the spectral width for the system of interest is large, however, this would necessitate using a small τ_t, where the smallest τ_t is $\tau_t \approx t_p$ (i.e., when $\tau = 0$). In this case, the selectivity or width of the excitation spectrum about $\nu_Z = 0$ Hz is approximately given by $\frac{1}{N\tau_t}$, which for $\tau_t \approx t_p$ means that the selectivity is roughly proportional to $\frac{1}{Nt_p} = \frac{2\pi\nu_{RF}}{\Theta}$. In this limit, the effect of the DANTE sequence is similar to evolution under continuous RF irradiation, which leads to a very broad excitation profile unless ν_{RF} is weak or $\Theta \gg 2\pi$. Under these conditions, the DANTE sequence is equivalent to applying a long, low-amplitude RF pulse.

As mentioned in the introduction, an alternative way to excite only a single resonance using a DANTE-like sequence would be to violate the periodicity of the DANTE sequence. This could be accomplished in a variety of ways, for example, such as using aperiodic delays, modulating the pulse amplitudes and delays,

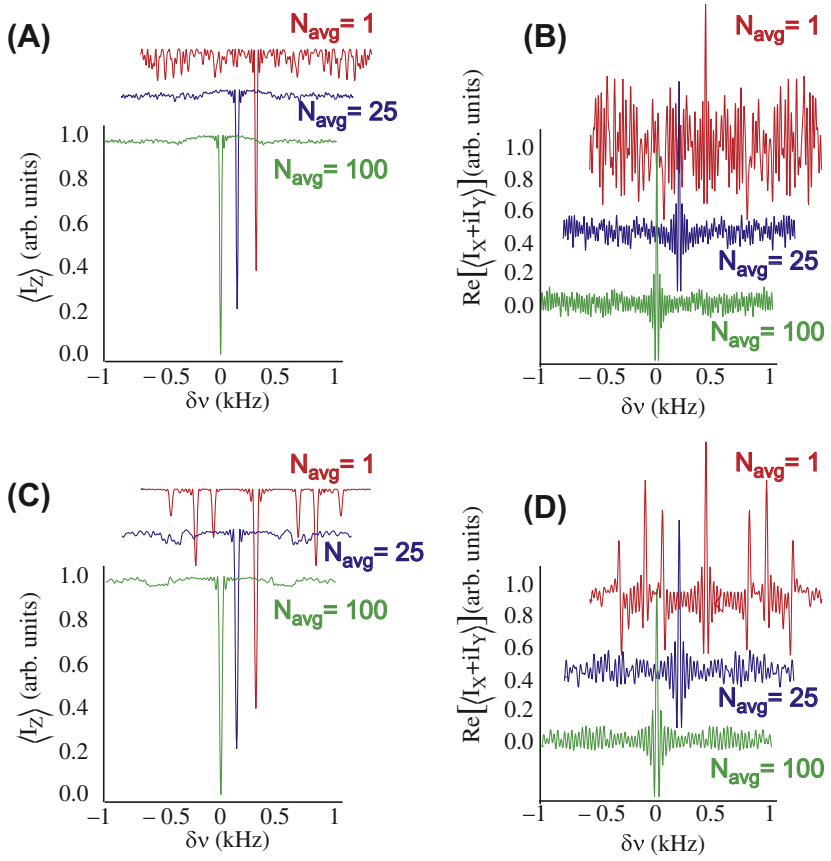

Fig. 4. (Color online) Theoretically calculated excitation [(B) and (D)] and $\hat{z}$-magnetization profiles [(A) and (C)] for a series of p-DANTE sequences (Fig. 1B). In all p-DANTE sequences, $N = 30$, $\theta = \frac{\pi}{60}$, and $\phi_k = 0$ for all k so that only spins resonating at $\nu_{\mathrm{sel}} = 0$ Hz [$\delta\nu = \nu_Z - \nu_{sel} = 0$ Hz] are rotated about the $\hat{x}$-axis by $\Theta = \frac{\pi}{2}$. In (A) and (B), one hundred different p-DANTE sequences with randomly chosen delays were generated such that the average pulse delay, $\frac{1}{29}\sum_{k=1}^{29}\tau_k = 1.6$ ms, was the same for all p-DANTE sequences. The excitation and $\hat{z}$-magnetization profiles were averaged over N_{avg} different p-DANTE sequences with $N_{\mathrm{avg}} = 1$ (red curve), $N_{\mathrm{avg}} = 25$ (blue curve), and $N_{\mathrm{avg}} = 100$ (green curve). In (C) and (D), one hundred different p-DANTE sequences with periodically modulated delays were used, where the kth delay for the pth experiment was $\tau_k^p = \tau_p\left[1 + \frac{\delta\tau}{\tau}\cos\left(\frac{2\pi k}{f_p}\right)\right]$, where $\frac{\delta\tau}{\tau} = \frac{1}{\sqrt{2}}$ and f_p was inversely proportional to the square root of the pth prime number (e.g., $f_1 = 1/\sqrt{2}, f_2 = 1/\sqrt{3}$, up to $f_{100} = 1/\sqrt{541}$). The time τ_p was chosen to ensure that the averaged delay was the same for all p and was also the same as that used in Fig. 4A and B for randomly chosen delays, i.e., $\frac{1}{29}\sum_{k=1}^{29}\tau_k^p = 1.6$ ms for all p. The averaged excitation and $\hat{z}$-magnetization profiles for $N_{\mathrm{avg}} = 1$ [red curve with $f_1 = 1/\sqrt{2}$], $N_{\mathrm{avg}} = 25$ [blue curve, averaging from $f_1 = 1/\sqrt{2}$ to $f_{25} = 1/\sqrt{97}$], and $N_{\mathrm{avg}} = 100$ [green curve, averaging from $f_1 = 1/\sqrt{2}$ to $f_{100} = 1/\sqrt{541}$] are shown. As N_{avg} increases, the "fluctuations" in both $\langle I_Z\rangle$ and $-\langle I_Y\rangle$ decrease. For $N_{\mathrm{avg}} = 100$, the resulting excitation and $\hat{z}$-magnetization profiles for p-DANTE sequences using randomly chosen delays (A and B) and those using periodically modulated delays (C and D) were practically identical.

pulse sculpting the θ-pulses [20,21]. One particular class of aperiodic DANTE sequences that is considered in this paper, pseudorandom-DANTE (p-DANTE), is illustrated in Fig. 1B, where N small-flip θ-pulses are applied with a delay of τ_k between the kth and $(k+1)$th pulse, where in general, $\tau_k \neq \tau_j$. For such a sequence to selectively and efficiently excite spins at a single resonance frequency ν_{sel}, the phases of the θ-pulses must be modulated and correlated with the interpulse delays. For p-DANTE excitation at ν_{sel}, the phase of the $(k+1)$th pulse is given by $\phi_{k+1} = -2\pi\nu_{sel}\left(kt_p + \sum_{j=1}^{k}\tau_j\right) = -2\pi\nu_{sel}T_k$, where $T_k = kt_p + \sum_{j=1}^{k}\tau_j$, and $\phi_1 = 0$ and $T_0 = 0$.

As in the DANTE case, the propagator for the p-DANTE sequence can be written as $\widehat{U}(T_{tot}) = \widehat{U}_{free}(\omega_Z T_{tot})\exp\left(-\frac{i}{\hbar}\overline{H}_{avg}Nt_p\right)$, where $T_{tot} = T_{N-1} + t_p = Nt_p + \sum_{j=1}^{N-1}\tau_j$, and $\overline{H}_{avg}$ is the average Hamiltonian for the p-DANTE sequence with the first two terms of $\overline{H}_{avg}$ given by:

$$\begin{aligned}\frac{\overline{H}^{(1)}_{avg}}{\hbar} &= \frac{1}{N}\sum_{k=0}^{N-1}\widehat{U}^{\dagger}_{free}(\Delta\omega T_k)\left(\frac{\overline{H}^{(1)}_{p,0}+\overline{H}^{(2)}_{p,0}}{\hbar}\right)\widehat{U}_{free}(\Delta\omega T_k)\\ &= \frac{a}{N}\sum_{k=1}^{N}\left(\widehat{I}_+e^{i\left(\Delta\omega T_k+\frac{\omega_Z t_p}{2}\right)} + I_-e^{-i\left(\Delta\omega T_k+\frac{\omega_Z t_p}{2}\right)}\right) + b\widehat{I}_Z \end{aligned} \tag{14}$$

$$\begin{aligned}\frac{\overline{H}^{(2)}_{avg}}{\hbar} &= \frac{t_p}{2iN\hbar^2}\sum_{k>j}\Big[\widehat{U}^{\dagger}_{free}(\Delta\omega T_k)\left(\overline{H}^{(1)}_{p,0}+\overline{H}^{(2)}_{p,0}\right)\widehat{U}_{free}(\Delta\omega T_k),\\ &\quad \widehat{U}^{\dagger}_{free}(\Delta\omega T_j)\left(\overline{H}^{(1)}_{p,0}+\overline{H}^{(2)}_{p,0}\right)\widehat{U}_{free}(\Delta\omega T_j)\Big]\\ &= \frac{t_p}{2iN}\sum_{k>j}\left[\frac{a}{2}\left(e^{i\Delta\omega\left(T_k+\frac{t_p}{2}\right)}\widehat{I}_+ + e^{-i\Delta\omega\left(T_k+\frac{t_p}{2}\right)}\widehat{I}_-\right)\right.\\ &\quad \left.+b\widehat{I}_Z,\frac{a}{2}\left(e^{i\Delta\omega\left(T_j+\frac{t_p}{2}\right)}\widehat{I}_+ + e^{-i\Delta\omega\left(T_j+\frac{t_p}{2}\right)}\widehat{I}_-\right) + b\widehat{I}_Z\right]\\ &= \frac{t_p ab}{4iN}\sum_{k>j}(e^{i\Delta\omega T_j}-e^{i\Delta\omega T_k})e^{i\frac{\Delta\omega t_p}{2}}\widehat{I}_+ - (e^{-i\Delta\omega T_j}-e^{-i\Delta\omega T_k})e^{-i\frac{\Delta\omega t_p}{2}}\widehat{I}_-\\ &\quad + \frac{a^2t_p}{4iN}\sum_{k>j}(e^{i\Delta\omega(T_k-T_j)}-e^{i\Delta\omega(T_j-T_k)})\widehat{I}_Z\\ &= \frac{abt_p}{2N}\left[\sum_{k>j}\sin\left(\frac{\Delta\omega(T_j-T_k)}{2}\right)\left(\widehat{I}_+e^{i\Delta\omega\left(\frac{T_j+T_k+t_p}{2}\right)} + \widehat{I}_-e^{-i\Delta\omega\left(\frac{T_j+T_k+t_p}{2}\right)}\right)\right]\\ &\quad + \frac{a^2t_p}{2N}\widehat{I}_Z\sum_{k>j}\sin(\Delta\omega(T_k-T_j)) \end{aligned} \tag{15}$$

where $\Delta\omega = 2\pi(\nu_Z - \nu_{sel}) = 2\pi\delta\nu$, and a and b were previously defined in Eq. (9). Unlike the DANTE case, the average delay between pulses fluctuates within the p-DANTE sequence, that is, $\frac{T_k}{k} \neq \frac{T_j}{j}$ for $k \neq j$. For $\delta\nu \neq 0$ Hz, a p-DANTE sequence is effectively equivalent to applying an RF field with a fluctuating offset (Fig. 2A), the result of which is a seemingly random excitation profile for those spins with $\delta\nu \neq 0$ Hz. Spins with $\delta\nu = 0$ Hz are rotated by $N\theta = \Theta$. This is illustrated by the theoretical calculations shown in Fig. 4A and B for the excitation and $\hat{z}$-magnetization profiles, averaged over (up to $N_{avg} = 100$) different p-DANTE sequences, respectively. For all p-DANTE sequences in Fig. 4, $N = 30$ and the various 29 τ_k's were chosen randomly but were scaled to ensure that the average delay time in each p-DANTE sequence was the same, $\frac{1}{29}\sum_{k=1}^{29}\tau_k = 1.6$ ms. Consider the excitation and $\hat{z}$-magnetization profile for a single p-DANTE sequence [red curve ($N_{avg} = 1$)] shown in Fig. 4A and B. A maximum rotation of $\Theta = \frac{\pi}{2}$ occurs at $\delta\nu = 0$ Hz, where $-\langle\widehat{I}_Y\rangle = 1$ and $\langle\widehat{I}_Z\rangle = 0$. Away from $\delta\nu = 0$ Hz, the excitation and $\hat{z}$-magnetization profiles are quite noisy, but $|\langle\widehat{I}_Y\rangle| < 1$ and $\langle\widehat{I}_Z\rangle > 0$. Note that the $\hat{z}$-magnetization profile is less noisy than the excitation profile since rotations away from the $\hat{z}$ direction go as $\cos(\theta) \approx 1 - \frac{\theta^2}{2}$, whereas excitations go as $\sin(\theta) \approx \theta$ for $\theta \ll 1$.

If the excitation and $\hat{z}$-magnetization profiles are averaged over different p-DANTE sequences that are selective for ν_{sel} and with the same total pulse length, then the fluctuations in both the excitation (Fig. 4B) and $\hat{z}$-magnetization (Fig. 4B) profiles for $\delta\nu \neq 0$ roughly decrease as $\frac{1}{\sqrt{N_{avg}}}$ (at least initially) relative to the excitation at $\delta\nu = 0$ Hz. However, even when $N_{avg} \gg 1$, there still exists a "baseline" excitation at $\delta\nu \neq 0$ Hz that is nonzero (averaging simply decreases the fluctuations about the baseline excitation). The average "baseline" excitation away from $\delta\nu = 0$ Hz but within the bandwidth of the RF pulses, $\frac{\omega_{RF}}{2\pi}$, is approximately given by $\overline{|\langle\widehat{I}_Y\rangle|} \approx \frac{N\theta}{N+2}$, which for $N \gg 2$ is approximately given by $\overline{|\langle\widehat{I}_Y\rangle|} \approx \theta$. This can be understood by the fact that the first θ-pulse is common to all p-DANTE sequences, whereas the effects of subsequent θ-pulses depend upon the delays and are, in a sense, averaged away as N_{avg} increases. The magnitude of the transverse magnetization away from $\delta\nu = 0$ Hz appears somewhat uniform, which can be seen in Fig. 4B. Finally, averaging over different p-DANTE sequences results in a decrease in the $\hat{z}$-magnetization profile for $\delta\nu \neq 0$ Hz within the RF bandwidth. In this case, the $\hat{z}$-magnetization profile is approximately given by $\overline{\langle\widehat{I}_Z\rangle} \approx 1 - \frac{(N+1)\theta^2}{2}$. This can be understood by the fact that the $\hat{z}$-magnetization before the θ-pulse is reduced by a factor of $\cos(\theta)$ after application of the θ-pulse. The transfer of transverse magnetization to $\hat{z}$-magnetization, averaged over different p-DANTE sequences, is approximately zero for $\delta\nu \neq 0$ Hz. Therefore, the "baseline" $\hat{z}$-magnetization is approximately given by $(\cos(\theta))^N \approx 1 - N\frac{\theta^2}{2}$ for $\theta \ll \frac{\pi}{3}$ and for $\delta\nu \neq 0$ Hz. Both excitation and deviations in $\hat{z}$-magnetization from unity for $\delta\nu \neq 0$ Hz decrease as $\theta \propto \frac{1}{N}$ for fixed $\Theta = N\theta$.

Besides randomly chosen delays, averaging over different sets of delays that are periodically modulated can also lead to selective excitation. Consider a series of delays, where the kth delay is given by $\tau_k = \tau + \delta\tau\cos\left(\frac{2\pi k}{f}\right)$ for $N-1 \geqslant k \geqslant 1$, where f is a real number, and $\tau \geqslant \delta\tau$ so that $\tau_k \geqslant 0$. For such a sequence to selectively excite spins resonating at ν_{sel}, the phase of the $(k+1)$th pulse must be given by $\phi_{k+1} = -2\pi\nu_{sel}T_k$, where:

$$\begin{aligned}T_k &= \sum_{j=1}^{k}\tau_j = \sum_{j=1}^{k}\tau + \frac{\delta\tau}{2}\left(e^{i\frac{2\pi j}{f}} + e^{-i\frac{2\pi j}{f}}\right)\\ &= k\tau + \frac{\delta\tau}{2}\left(\frac{e^{i\frac{(2k+1)\pi}{f}} - e^{i\frac{\pi}{f}}}{2i\sin\left(\frac{\pi}{f}\right)} - \frac{e^{-i\frac{(2k+1)\pi}{f}} - e^{-i\frac{\pi}{f}}}{2i\sin\left(\frac{\pi}{f}\right)}\right)\\ &= k\tau - \frac{\delta\tau}{2}\left(1 - \csc\left(\frac{\pi}{f}\right)\sin\left(\frac{2k+1}{f}\pi\right)\right)\end{aligned} \tag{16}$$

with $T_0 = 0$. The total time for such a p-DANTE sequence is given by $T_{tot} = Nt_p + T_{N-1} = Nt_p + (N-1)\tau - \frac{\delta\tau}{2} + \frac{\delta\tau}{2}\csc\left(\frac{\pi}{f}\right)\sin\left(\frac{\pi(2N-1)}{f}\right)$.

Using the value of T_k in Eq. (16) and Eq. (A6) in Appendix A, $\overline{H}^{(1)}_{avg}$ in Eq. (14) can be evaluated and is given by:

$$\begin{aligned}\overline{H}^{(1)}_{avg} &= \frac{a}{2N}\sum_{k=0}^{N-1}\left(\widehat{I}_+e^{i\left(\Delta\omega T_k+\frac{\omega_Z t_p}{2}\right)} + I_-e^{-i\left(\Delta\omega T_k+\frac{\omega_Z t_p}{2}\right)}\right) + b\widehat{I}_Z\\ &= \frac{a}{2}\sum_{n=-\infty}^{\infty}J_n\left(\frac{\Delta\omega\delta\tau}{2}\csc\left(\frac{\pi}{f}\right)\right)\frac{\operatorname{sinc}\left(\frac{N(\Delta\omega\tau+2n\pi)}{2}\right)}{\operatorname{sinc}\left(\frac{\Delta\omega\tau+2n\pi}{2}\right)}\\ &\quad\times\left(I_+e^{i\chi_n} + I_-e^{-i\chi_n}\right) + b\widehat{I}_Z\end{aligned} \tag{17}$$

where J_n is a bessel function of order n, and $\chi_n = \Delta\omega\,\frac{(N-1)\tau-\delta\tau}{2} + \frac{Nn\pi}{f} + \frac{\omega_Z t_p}{2}$. From Eq. (17), $\overline{H}^{(1)}_{avg}$ is maximal at the conditions $\delta\nu = \frac{m}{\tau} - \frac{n}{f\tau}$ for integer m and n. These define the resonance

conditions for p-DANTE sequences with $\tau_k = \tau + \delta\tau\cos\left(\frac{2\pi k}{f}\right)$. However, $\overline{H}^{(1)}_{\rm avg}$ is scaled by $J_n\left(\left(m-\frac{n}{f}\right)\frac{\pi\delta\tau}{\tau}\csc\left(\frac{\pi}{f}\right)\right)$, which is less than one for $m \neq \frac{n}{f}$. If f is an irrational number, then the maximal scaling only occurs for the $m = n = 0$ resonance [$J_0(0) = 1$]. At all other resonance conditions, $J_n\left(\left(m-\frac{n}{f}\right)\frac{\pi\delta\tau}{\tau}\csc\left(\frac{\pi}{f}\right)\right)$ is less than one, resulting in a smaller overall rotation.

Fig. 4C and D show the numerically averaged $\hat{z}$-magnetization and excitation profiles respectively, averaged for up to one hundred different p-DANTE sequences using periodically modulated delays. In the simulations, $N = 30$ and $\frac{\delta\tau}{\tau} = \frac{1}{\sqrt{2}}$. For the pth p-DANTE sequence, f_p was set to be equal to the inverse of the square root of the pth prime number, i.e., $f_1 = 1/\sqrt{2}, f_2 = 1/\sqrt{3}$, up to $f_{100} = 1/\sqrt{541}$. The time τ_p for the pth p-DANTE experiment was chosen so that average interpulse delay, $\frac{1}{29}\sum_{j=1}^{29}\tau_j^p = 1.6$ ms, was the same as that used for the p-DANTE sequences with randomly chosen delays (Fig. 4A and B). Consider only a single p-DANTE sequence [$N_{\rm avg} = 1$ case (red curve) in which $f = \frac{1}{\sqrt{2}}$ and $\frac{1}{\tau} = 625.13$ Hz]. Unlike the case of using randomly chosen delays (red curves in Fig. 4A and B), where the resulting excitations appear randomly distributed throughout the spectral range, the excitation profile using periodically modulated delays occur at discrete $\delta\nu$ given by the resonance condition $\delta\nu = 625.13(m - \sqrt{2}n)$ Hz [Eq. (17)]. Note that while the resonance at $\delta\nu = 0$ ($m = 0$ and $n = 0$) is maximally excited [$\langle\hat{I}_Z\rangle = 0, \left|\langle\hat{I}_Y\rangle\right| = 1$], the degree of excitation at other resonance conditions is less. In particular, the resonances at $\delta\nu = \pm 625.13$ Hz ($m = \pm 1, n = 0$) are not observed in the calculated profile, since at these conditions, $\overline{H}^{(1)}_{\rm avg}$ is scaled by $J_0(-2.3046) = 0.053$, whereas the resonances at $\delta\nu = \pm 366.2$ Hz ($n = \mp 1$ and $m = \pm 2$) are clearly observed [$|J_1(1.35)| = 0.5325$]. As was the case for p-DANTE sequences using randomly chosen delays, averaging over different sets of periodically modulated p-DANTE sequences reduces the excitation everywhere except at $\delta\nu = 0$ Hz, which is a common resonance for all p-DANTE sequences used in Fig. 4. This is illustrated by comparing Fig. 4A and B with C and D. Fig. 4 for $N_{\rm avg} = 100$, where the $\hat{z}$-magnetization and excitation profiles for both periodically-modulated and randomly chosen delays appear essentially identical. Thus, averaging over aperiodic series of θ-pulses, where the delays are deterministically generated, results in excitation profiles that are similar to excitation profiles for randomly generated delays. This similarity is the reason behind the use of the moniker pseudorandom-DANTE for the sequence shown in Fig. 1B.

Finally, it should be noted that the conditions under which the average Hamiltonian in Eq. (17) provides a valid description of the p-DANTE sequence are approximately the same as those found for the DANTE sequence (Fig. 3). Fig. 5 shows the difference in the excitation (Fig. 5A) and $\hat{z}$-magnetization (Fig. 5B) profiles calculated using either the exact propagator or the propagator calculated using the average Hamiltonian up to second-order [Eqs. (15) and (17)] for the p-DANTE sequences used in Fig. 4C and D. As shown in Fig. 3, AHT works well for all $\delta\nu$ except slightly above and below the resonance conditions, $\delta\nu = \frac{m}{\tau} - \frac{n}{f\tau}$, which is evident from Fig. 5 for the $N_{\rm avg} = 1$ curve. The magnitude of the error from using $\overline{H}_{\rm avg}$ up to second-order is the same as that found for a DANTE sequence with $\Theta = \pi/2$. The agreement between the AHT calculations with the exact calculations appears to improve upon averaging over different p-DANTE sequences, except above and below the $\delta\nu = 0$ Hz, which is a common resonance for all p-DANTE sequences used in Fig. 5.

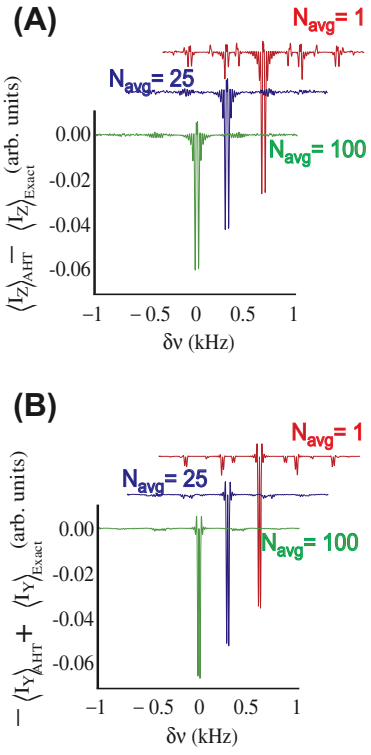

Fig. 5. (Color online) Difference in the (A) $\hat{z}$-magnetization and (B) excitation profiles for the p-DANTE sequences used in (C) and (D) calculated using the propagator from AHT, $\widehat{U}_{\rm AHT}(T_{\rm tot}) = \widehat{U}_{\rm free}(\omega_Z T_{\rm Tot})e^{-\frac{i}{\hbar}\left(\overline{H}^{(1)}_{\rm avg}+\overline{H}^{(2)}_{\rm avg}\right)Nt_p}$ [Eqs. (14) and (15)] versus the profiles calculated using the exact propagator, $\widehat{U}_{\rm exact}(T_{\rm tot})$. The agreement is relatively good over a wide frequency range except above and below the $\delta\nu = 0$ Hz resonance condition, $\delta\nu \approx \pm\frac{3\theta}{5\Theta\tau_i} = \pm 13$ Hz. For all $|\delta\nu| \gg \frac{3\theta}{5\Theta\tau_i}$ and $|\delta\nu| \ll \frac{3\theta}{5\Theta\tau_i}$, the agreement between AHT and the exact calculation improves with averaging over different p-DANTE sequences.

3. Experimental

All experiments were performed on a 300 MHz Avance Bruker spectrometer (static magnetic field of 7 T and an operating frequency for ^1H of 300.13 MHz), using a 5-mm Bruker BBO probe. A 2 M solution of acetone in acetone-d_6 was used to experimentally determine the excitation and $\hat{z}$-magnetization profiles as a function of frequency offset from the acetone resonance for both DANTE and two pseudorandom pulse sequences. The carrier frequency was changed in increments of 10 Hz over the frequency range [−580 Hz + $\nu_{\rm acetone}$, 580 Hz + $\nu_{\rm acetone}$] in order to experimentally determine the excitation and $\hat{z}$-magnetization profiles, resulting in a total of 1161 measurements. In order to measure the $\hat{z}$-magnetization, a $\frac{\pi}{2}$ pulse $\left[\frac{\omega_{RF}}{2\pi} = 21.4\ \text{kHz}\right]$ applied after the DANTE and p-DANTE sequences was phase cycled in concert with the receiver phase so that only the $\hat{z}$-magnetization prior to the last $\frac{\pi}{2}$ pulse was measured. A delay of 40 s was used between scans in all experiments in order to ensure that the system had relaxed back to equilibrium to avoid any distortions in the observed profiles (Fig. 6), and four scans were performed for each measurement. In all of these experiments, the integral of the acetone peak was measured. This was due to the fact that even though a BBO probe was used, radiation damping effects could not be ignored for the 2M acetone solution *after* application of the DANTE and p-DANTE sequences. The observed radiation time constant for the 2M acetone solution was $\tau_{RD} = 200$ ms. While radiation damping could be safely ignored during the DANTE and p-DANTE sequences, which all had a pulse sequence length of approximately 58 ms, radiation damping after the initial excitation resulted in the rotation of the acetone magnetization back to the $+\hat{z}$-axis, thereby causing distortions in the observed acetone signal. To correct for this, the integral of the acetone signal was calculated since it is invariant to radiation damping and serves as a good measure of the initial transverse magnetization after application of the RF

pulses. Furthermore, neglecting radiation damping during the experimental DANTE and p-DANTE sequences was a reasonable approximation for this sample since there was good agreement between theory [blue] and experiment [red] as shown in Fig. 6.

Finally, in order to demonstrate the improved selectivity in the excitation and $\hat{z}$-magnetization profiles by signal averaging over different p-DANTE sequences (as illustrated in Fig. 4), experiments using different p-DANTE sequences were performed on a solution of acetone, dimethyl sulfoxide (DMSO), and water diluted in D_2O, with [acetone] = 0.33 M, [DMSO] = 0.37 M, and [H_2O] = 0.53 M. All chemicals were obtained from Sigma-Aldrich.

4. Results and discussion

The experimentally determined excitation and $\hat{z}$-magnetization profiles under DANTE and two different p-DANTE sequences obtained using a 2M acetone solution in acetone-d_6 are shown in Fig. 6, where the blue and red curves correspond to the theoretical and experimental profiles, respectively. In these experiments, $N = 30$, $\theta = \frac{\pi}{60}$, and $t_p = 720$ ns were used with a maximum rotation of $\Theta = N\theta = \frac{\pi}{2}$. For the DANTE sequence, $\tau = 2$ ms. Over the spectral range shown in Fig. 6A and D, DANTE excitations at frequencies $\delta\nu = \pm\frac{1}{\tau} = \pm 500$ Hz and at $\delta\nu = 0$ Hz were observed. For

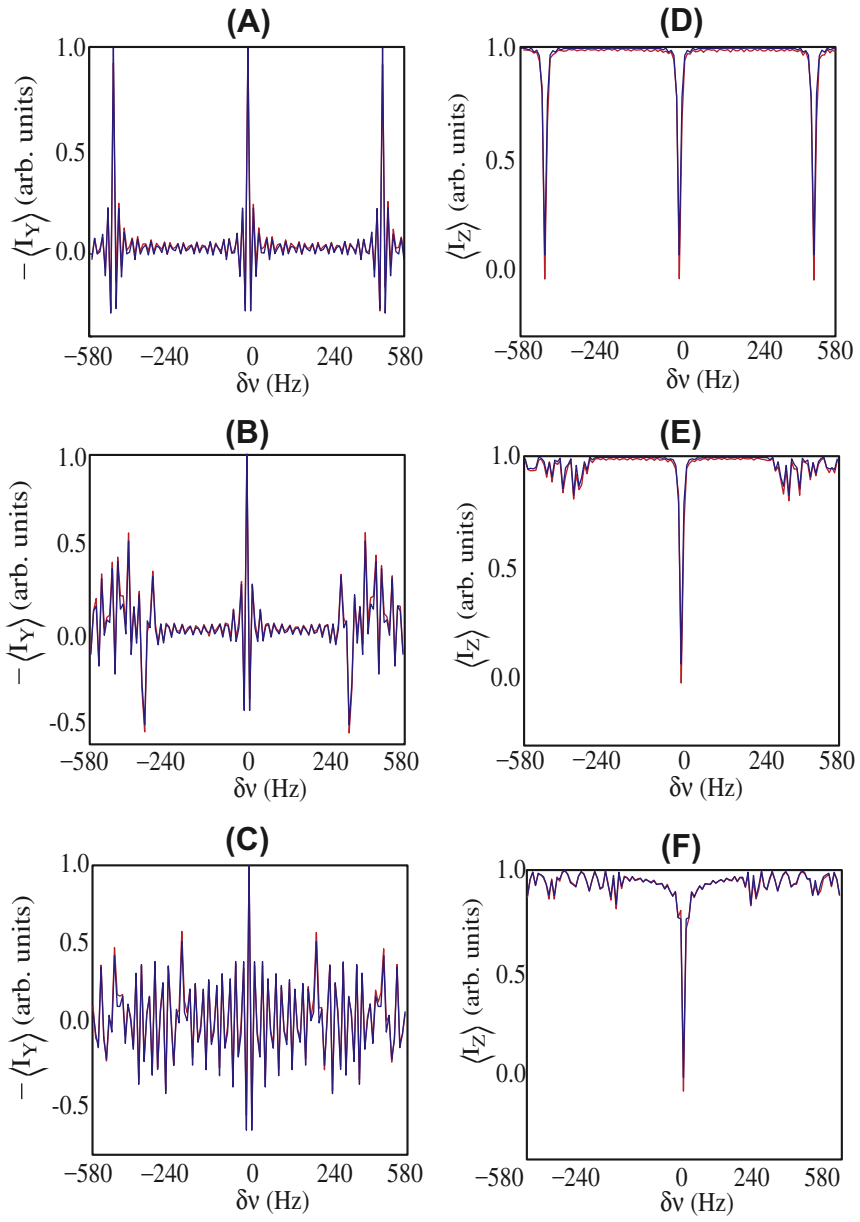

Fig. 6. (Color online) Experimental (red) and theoretical (blue) excitation (A–C) and $\hat{z}$-magnetization (D–F) profiles after application of the DANTE (A and D) and p-DANTE sequences (B, E, C, and F) as a function of the frequency offset from the acetone resonance, $\delta\nu = \nu - \nu_{\text{acetone}}$. In all experiments, $N = 30$ and $\theta = \frac{\pi}{60}$. The profiles were generated using a 2M acetone solution in acetone-d_6 by changing the RF carrier frequency from −580 Hz to 580 Hz in 10 Hz increments, and the resulting acetone resonance was integrated. For the DANTE sequence, $\tau = 2$ ms; with these parameters, the acetone resonance was maximally excited at $\delta\nu \approx \pm\frac{1}{\tau} = \pm 500$ Hz and at $\delta\nu = 0$ Hz over the spectral range [−580 Hz, 580 Hz]. For the p-DANTE sequences, the kth delay was either given by $\tau_k = 2.096\left[1 + \frac{1}{3}\cos\left(\frac{2k\pi}{23}\right)\right]$ ms (B and E) or by a UDD-like [11] delay $\tau_k = 2.063\left[1 - \cos\left(\frac{k\pi}{29+1}\right)\right]$ ms = $4.126\sin^2\left(\frac{k\pi}{2(29+1)}\right)$ (C and F). In both cases, the average delay between pulses was $\frac{1}{29}\sum_{k=1}^{29}\tau_k = 2$ ms in order to better compare the results with those obtained from the DANTE sequence shown in (A) and (D). For both p-DANTE sequences, there is minimal excitation at $\delta\nu = \pm 500$ Hz, although the UDD-like sequence (C and F) appears to generate smaller excitations over a wider frequency range than the other p-DANTE sequence (B and E). In all cases, there is good agreement between theory (blue) and experiment (red).

the p-DANTE sequences, the kth delay was given by either (Fig. 6C and F) $\tau_k = 2.063\left[1-\cos\left(\frac{k\pi}{29+1}\right)\right]$ ms $= 4.126\sin^2\left(\frac{k\pi}{2(29+1)}\right)$ [which is a similar set of delays used in a Uhrig Dynamical Decoupling (UDD) sequence [11]] or (Fig. 6B and E) $\tau_k = 2.096\left[1+\frac{1}{3}\cos\left(\frac{2k\pi}{23}\right)\right]$ ms. In both cases, the average delay between pulses was equal to $\frac{1}{29}\sum_{k=1}^{29}\tau_k = 2$ ms in order to allow for better comparison with the DANTE sequence used in Fig. 6A and D. Both p-DANTE sequences generated a maximum excitation ($\Theta = \frac{\pi}{2}$) at $\delta\nu = 0$ Hz, and, as expected, smaller excitations for $\delta\nu \neq 0$ Hz were also observed. Note that for p-DANTE sequence with UDD-like delays (Fig. 6C and F), the excitation and $\hat{z}$-magnetization profiles look similar to that of a p-DANTE sequence using randomly chosen delays (the red curve in Fig. 4A and B), whereas excitations using the other p-DANTE sequence (Fig. 6B and E) appear to be concentrated within a smaller frequency range.

In order to examine the effects of averaging over different p-DANTE sequences, experiments were performed on a DMSO/acetone/water solution in D_2O. The spectrum of the solution after a simple $\frac{\pi}{2}$-acquire sequence is shown in Fig. 7A, where the RF was applied on resonance with respect to the water signal [$\delta\nu_{\text{acetone,water}} = \nu_{\text{acetone}} - \nu_{\text{water}} = -768$ Hz and $\delta\nu_{\text{DMSO,water}} = \nu_{\text{DMSO}} - \nu_{\text{water}} = -620.2$ Hz]. The experimental excitation and $\hat{z}$-magnetization weighted spectra after application of the DANTE sequence with $N = 30$, $\theta = \frac{\pi}{60}$ ($t_p = 630$ ns), and $\tau \approx \frac{1}{|\delta\nu_{\text{DMSO,water}}|} =$ 1.6 ms are shown in Fig. 7B and C respectively. With $\tau = 1.6$ ms, the DANTE sequence efficiently excites both the water [$\delta\nu = \frac{0}{\tau} = 0$ Hz] and the DMSO [$\delta\nu = -\frac{1}{\tau} = -620$ Hz] resonances (Fig. 7B) but leaves the acetone magnetization mostly about the $\hat{z}$-axis (Fig. 7C).

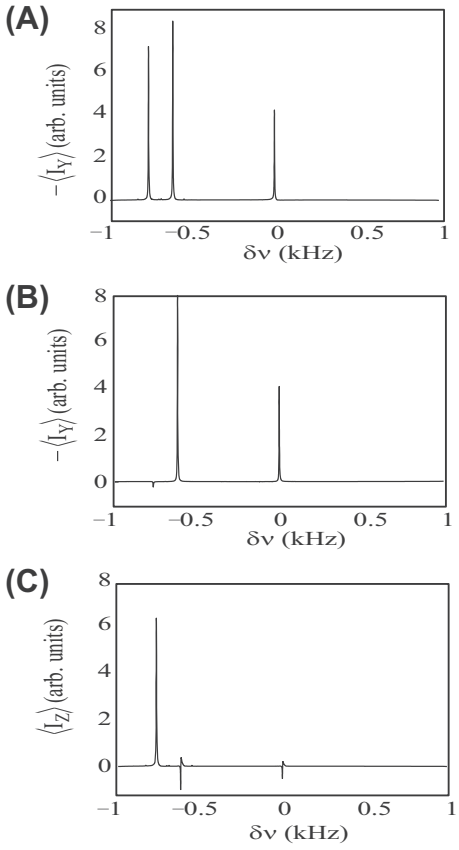

Fig. 7. (A) The spectrum after a $\frac{\pi}{2}$-acquire experiment for a DMSO, acetone, and water solution. The spectrum is centered on the water resonance [$\delta\nu = 0$ Hz]. (B) The spectrum after application of a DANTE pulse sequence with $N = 30$, $\theta = \frac{\pi}{60}$, $\Theta = N\theta = \frac{\pi}{2}$, and $\tau = \frac{1}{|\delta\nu_{\text{DMSO,water}}|} \approx 1.6$ ms. In this case, both the water and DMSO resonances were excited, whereas very little excitation occurred at the acetone resonance [$\delta\nu_{\text{acetone,water}} = -768$ Hz]. (C) The $\hat{z}$-magnetization weighted spectrum after application of the DANTE pulse sequence. As expected from (B), there was substantial $\hat{z}$-magnetization for the acetone resonance and little $\hat{z}$-magnetization for both the water and DMSO resonances after application of the DANTE sequence.

The averaged excitation (Fig. 8B) and $\hat{z}$-magnetization weighted spectra (Fig. 8A) for the DMSO/acetone/water solution were obtained using up to one hundred different p-DANTE sequences, and the results are shown for $N_{\text{avg}} = 1$ [red curve], $N_{\text{avg}} = 25$ [blue curve], and $N_{\text{avg}} = 100$ [green curve] in Fig. 8. The p-DANTE sequences used in Fig. 8 were the same used in the theoretical calculations shown in Fig. 4C and D, where the kth delay used in p^{th} experiment was given by $\tau_k^p = \tau_p\left(1+\frac{\delta\tau_p}{\tau_p}\cos\left(\frac{2\pi k}{f_p}\right)\right) = \tau_p\left(1+\frac{1}{\sqrt{2}}\cos\left(\frac{2\pi k}{f_p}\right)\right)$ for $k = 1$ to $k = N-1 = 29$. In each experiment, τ_p was chosen such that the total time of the delays was the same as that used in the DANTE sequence shown in Fig. 7B and C, i.e., $\sum_{j=1}^{29}\tau_j^p = T_{29}^p = 46.77$ ms $\approx 29\times 1.6$ ms. Using Eq. (16) along with $T_{29}^p = 46.77$ ms, τ_p can be determined for the pth experiment. Therefore, the actual time for the k^{th} delay in the pth experiment was given by:

$$\tau_k^p = \frac{46.77\text{ ms}}{29-\frac{1}{2\sqrt{2}}\left(1-\csc\left(\frac{\pi}{f_p}\right)\sin\left(\frac{59\pi}{f_p}\right)\right)}\left(1+\frac{1}{\sqrt{2}}\cos\left(\frac{2\pi k}{f_p}\right)\right) \qquad (18)$$

As in Fig. 4C and D, the water resonance ($\delta\nu = 0$ Hz) was maximally excited, whereas the averaged excitation at both the acetone and DMSO resonances decreased upon averaging over different p-DANTE sequences. From Fig. 8B, averaging over different p-DANTE sequences did not generate any distortions in the amplitude and phase of the water resonance. Similarly, the $\hat{z}$-magnetization weighted spectra indicated that the acetone and DMSO magnetization remained mostly about the $\hat{z}$-axis after application of the p-DANTE sequence, whereas there was little $\hat{z}$-magnetization at the water resonance.

Finally, it is useful to compare the p-DANTE selective excitation scheme with traditional selective pulses. The selectivity of both traditional selective pulses and p-DANTE excitation is determined by the total length of the pulse, T_{tot}, with the excitation bandwidth about ν_{sel} being inversely proportional to T_{tot}. However, traditional shaped selective pulses generate a well-defined excitation profile after a single application of the pulse, whereas p-DANTE selective excitation only achieves this selectivity after averaging over different p-DANTE sequences (see Fig. 4) to reduce spurious excitations away from ν_{sel}. With regards to this aspect, p-DANTE sequences do not offer an advantage over traditional selective pulses for use in traditional NMR experiments. However, for experiments performed in non-laboratory settings, where shaped or phase modulated pulses are not readily available, such as in NMR logging experiments [32] or experiments using the NMR-mouse [30,31], p-DANTE sequences provide a convenient method to selectively excite a single resonance ($\nu_{\text{sel}} = 0$ Hz) without the need for amplitude/phase modulation. Furthermore, modifications of the p-DANTE sequences to selectively excite particular multiple-quantum transitions (MQ-DANTE) benefit from averaging over multiple sets of delays in order to reduce spurious excitations for other MQ-transitions, which will be presented elsewhere. Finally, it should be noted that colored noise sequences for selective excitation in imaging applications [16] have been developed, which were valid within the linear response regime $[\Theta \ll \frac{\pi}{3}]$.

Since selectivity is ultimately determined by T_{tot}^{-1}, high selectivity requires long pulse times which means that relaxation effects cannot be neglected. In the absence of RF irradiation, T_1 (longitudinal) and T_2 (transverse) determine the relevant relaxation timescales during periods of free evolution. However, the effective

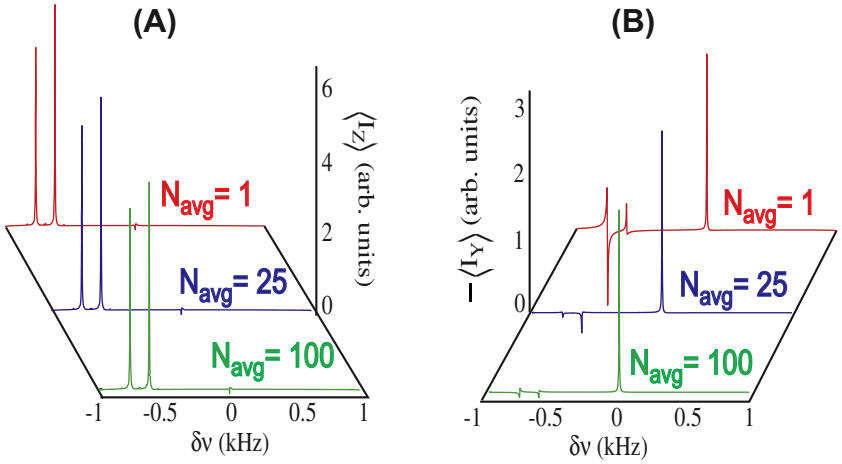

Fig. 8. (Color online) Experimental stacked plots of the (A) $\hat{z}$-magnetization weighted spectra and the (B) excitation spectra after averaging over N_{avg} = 1 (red), N_{avg} = 25 (blue), and N_{avg} = 100 (green) p-DANTE sequences (same sequences used in Fig. 4C and D) applied to the acetone, DMSO, and water solution used in Fig. 7. From Fig. 4C and D, only the water resonance at $\delta\nu$ = 0 Hz should be efficiently excited. From Fig. 6B the water resonance [$\delta\nu$ = 0 Hz] is efficiently excited without any distortion in phase or amplitude with averaging over different p-DANTE sequences, and the amount of excitation at the acetone and DMSO resonances decreases as N_{avg} increases. In Fig. 8A, the $\hat{z}$-magnetization weighted spectra are shown, illustrating that both the acetone and DMSO magnetization lie mostly along the $\hat{z}$-direction after application of the p-DANTE sequences.

relaxation timescales during a shaped pulse can be quite different than the T_1 and T_2 times during free evolution, and these timescales can depend quite sensitively upon the particular sample being measured along with the particular selective pulse being applied [33]. For the p-DANTE sequence, as long as the average interpulse delay is much greater than the time of the θ-pulse, T_1 and T_2 remain the relevant relaxation timescales, independent of sample. It should also be noted that for the sequences used in Figs. 6–8, $T_{tot} \approx 59$ ms, whereas $T_1, T_2 \approx$ s. Therefore, relaxation during these p-DANTE sequences could be safely ignored. Finally, one particular advantage of the p-DANTE (and DANTE) sequences compared to other selective pulses is that the mechanism of p-DANTE's selectivity is relatively straightforward, enabling these pulses to be easily designed and implemented, whereas the mechanism behind the selectivity of many shaped pulses, such as E-BURP [34], is not as clear, especially in the nonlinear regime $\left[\Theta > \frac{\pi}{3}\right]$. Furthermore, since ν_{sel} is determined by the phase-modulation of the θ-pulses in a p-DANTE sequence, interleaving the θ-pulses between shaped, pulsed-field gradients makes the apparent phase-modulation spatially dependent, thereby making the selectivity of the p-DANTE sequence spatially dependent, i.e., $\nu_{sel}(\vec{r})$. Such sequences could therefore have applications in ultrafast NMR experiments [35,36].

5. Conclusions

In this work, average Hamiltonian theory (AHT) was used to calculate the effective propagators for the DANTE (Fig. 1A) and pseudorandom-DANTE or p-DANTE (Fig. 1B) sequences. An AHT (up to second-order) description of the DANTE sequence was found to be valid for overall rotations of $\Theta \leqslant \frac{5\pi}{9}$ for all frequencies. For larger rotations $\left[\Theta \geqslant \frac{5\pi}{9}\right]$, the AHT description of the DANTE sequence was also found to be valid except for frequencies slightly above and below integer multiples of the DANTE frequency, $\frac{1}{\tau_t}$, where $\tau_t = \tau + t_p$, τ is the interpulse delay, and t_p is time of the θ-pulse. With these restrictions in mind, an AHT description for the p-DANTE sequence (Fig. 1B) was developed, where modulations in the interpulse delay introduce an aperiodicity to the sequence so that only a single frequency, ν_{sel}, is excited. While the excitation and $\hat{z}$-magnetization profiles for a single p-DANTE sequence are not particularly clean, i.e., small excitations exist at $\nu_Z \neq \nu_{sel}$, averaging over different p-DANTE sequences "cleans up" the excitation profiles so that only a small baseline excitation exists everywhere except at ν_{sel}, where the magnetization is maximally rotated by Θ. Experimental demonstrations (Figs. 6 and 8) of the p-DANTE sequences were found to be in good agreement with AHT predictions. Finally, since any shaped pulse can be recast into a DANTE-like sequence with nonconstant delays/flip-angles/phases [25–27], the AHT description presented in this paper could provide insight into pulse shaping/sculpting and selective excitation in both NMR and optical spectroscopies.

For future work, determining the optimal set of p-DANTE sequences that generate the "cleanest" excitation profiles with the smallest number of p-DANTE sequences will be investigated. Since the frequency selection in p-DANTE sequences is determined by correlating the pulse phases with the delays, the p-DANTE sequences could also be incorporated into ultrafast NMR [35,36] techniques to selectively excite resonances within different parts of the sample volume. Furthermore, extending the AHT results obtained in this paper to coupled spin systems is currently underway, whereby DANTE-like or p-DANTE-like sequences can be used to selectively excite multiple-quantum spin transitions. The conditions under which an AHT description can be applied in these systems are approximately the same as those found in this paper, since any subspace of two transitions can be described [37] as an effective spin-1/2, and the theory presented in this work can be used to derive analytical expressions for the average Hamiltonian in simple coupled spin systems. Coupling these techniques with ultra-fast NMR should enable the quick determination of all spin transitions in a given molecular system. Finally, the theory presented in this work would also be applicable to describing the evolution under a series of imperfect $n\pi$ pulses $\left[n\pi + \theta \text{ with } \theta \ll \frac{\pi}{3}\right]$ and could be modified to investigate imperfections in quantum bang-bang [12,38] techniques consisting of a series of π-pulses.

Acknowledgments

We would like to thank Alex Burum and Dr. John Logan for a careful reading of this manuscript. This work was supported by a Camille and Henry Dreyfus New Faculty award, and startup funds and a Provost Research award from the University of Miami.

Appendix A. Harmonic sums

In deriving $\overline{H}_{avg} \approx \overline{H}^{(1)}_{avg} + \overline{H}^{(2)}_{avg}$ for the DANTE sequence in Eqs. (11) and (12), explicit formulas for sums of $e^{ik\omega\tau_t}$ over integer k

were used. In this section, the relevant formula for these sums are derived.

The sum, $\sum_{k=0}^{N-1} e^{\pm ikf} = \sum_{k=0}^{N-1} (e^{\pm if})^k$, is nothing more than a geometric series of $e^{\pm if}$. Using the formula for a geometric series, $\sum_{k=0}^{N-1} c^k = \frac{c^N - 1}{c-1}$, gives:

$$\sum_{k=0}^{N-1} (e^{\pm if})^k = \frac{e^{\pm iNf} - 1}{e^{\pm if} - 1} = e^{\pm i\frac{(N-1)f}{2}} \frac{\sin\left(\frac{Nf}{2}\right)}{\sin\left(\frac{f}{2}\right)} = Ne^{\pm i\frac{(N-1)f}{2}} \frac{\operatorname{sinc}\left(\frac{Nf}{2}\right)}{\operatorname{sinc}\left(\frac{f}{2}\right)} \tag{A1}$$

For double sums of the form $\sum_{k>j} e^{\pm i(k-j)f}$ for $j = 0, 1, \ldots, N-2$ and $k = 1, 2, \ldots, N-1$, one has:

$$\begin{aligned}
\sum_{k>j} e^{\pm i(k-j)f} &= \sum_{k=1}^{N-1} e^{\pm ikf} + e^{\mp if} \sum_{k=2}^{N-1} e^{\pm ikf} + e^{\mp 2if} \sum_{k=3}^{N-1} e^{\pm ikf} + \ldots \\
&\quad + e^{\mp i(N-2)f} e^{\pm i(N-1)f} = e^{\pm i(N-1)f} + 2e^{\pm i(N-2)f} + 3e^{\pm i(N-3)f} \\
&\quad + \ldots + (N-1)e^{\pm if} = \sum_{k=1}^{N-1} ke^{\pm i(N-k)f} \\
&= \frac{e^{\pm iNf}}{\mp i} \frac{\partial \sum_{k=1}^{N-1} e^{\mp ikf}}{\partial f} = \frac{e^{\pm iNf}}{\mp i} \frac{\partial}{\partial f} \left(\frac{e^{\mp iNf} - 1}{e^{\mp if} - 1} - 1 \right) \\
&= \frac{1 - e^{\pm iNf} - N(1 - e^{\pm if})}{4\sin^2\left(\frac{f}{2}\right)}
\end{aligned} \tag{A2}$$

Therefore

$$\begin{aligned}
\sum_{k>j} e^{i(k-j)f} - e^{-i(k-j)f} &= \frac{N(e^{if} - e^{-if}) - (e^{iNf} - e^{-iNf})}{4\sin^2\left(\frac{f}{2}\right)} \\
&= \frac{i}{2} \frac{N\sin(f) - \sin(Nf)}{\sin^2\left(\frac{f}{2}\right)} \\
&= \frac{2iN}{f} \frac{\operatorname{sinc}(f) - \operatorname{sinc}(Nf)}{\operatorname{sinc}^2\left(\frac{f}{2}\right)}
\end{aligned} \tag{A3}$$

Another sum that is necessary in evaluating $\overline{H}^{(2)}_{\text{avg}}$ in Eq. (12) is

$$\begin{aligned}
\sum_{k>j} e^{\pm ikf} - e^{\pm ijf} &= \sum_{k=1}^{N-1} e^{\pm ikf} - (N-1) + \sum_{k=2}^{N-1} e^{\pm ikf} - (N-2)e^{\pm if} \\
&\quad + \ldots + e^{\pm i(N-1)f} - e^{\pm i(N-2)f} \\
&= \sum_{k=1}^{N-1} ke^{\pm ikf} - \sum_{k=1}^{N-1} (N-k)e^{\pm ikf} e^{\mp if} \\
&= (1 + e^{\mp if}) \sum_{k=1}^{N-1} ke^{\pm ikf} - Ne^{\mp if} \sum_{k=1}^{N-1} e^{\pm ikf} \\
&= \frac{(e^{\mp if} + 1)(e^{\pm if} - Ne^{\pm iNf} + (N-1)e^{\pm if(1+N)})}{(e^{\pm if} - 1)^2} \\
&\quad - \frac{N(e^{\pm i(N-1)f} - 1)}{e^{\pm if} - 1} \\
&= \mp \frac{i}{2} e^{\pm i\frac{N-1}{2}f} \\
&\quad \times \frac{(N-1)\sin\left(\frac{(N+1)f}{2}\right) - (1+N)\sin\left(\frac{(N-1)f}{2}\right)}{\sin^2\left(\frac{f}{2}\right)} \\
&= \mp \frac{i}{f} (N^2 - 1) e^{\pm i\frac{N-1}{2}f} \\
&\quad \times \frac{\operatorname{sinc}\left(\frac{(N+1)f}{2}\right) - \operatorname{sinc}\left(\frac{(N-1)f}{2}\right)}{\operatorname{sinc}^2\left(\frac{f}{2}\right)}
\end{aligned} \tag{A4}$$

Finally, a sum that is particularly useful for deriving $\overline{H}^{(1)}_{\text{avg}}$ in Eq. (17) for periodically modulated delays, $\tau_k = \tau + \delta\tau\cos\left(\frac{2\pi k}{f}\right)$ with $T_k = \sum_{j=1}^{k} \tau_j$ given by Eq. (16), is:

$$\begin{aligned}
\sum_{k=0}^{N-1} e^{\pm i\Delta\omega T_k} &= e^{\mp i\Delta\omega\frac{\delta\tau}{2}} \sum_{k=0}^{N-1} e^{\pm i\Delta\omega k\tau} e^{\pm i\frac{\Delta\omega\delta\tau}{2}\csc\left(\frac{\pi}{f}\right)\sin\left(\frac{2k+1}{f}\pi\right)} \\
&= e^{\mp i\Delta\omega\frac{\delta\tau}{2}} \sum_{k=0}^{N-1} e^{\pm i\Delta\omega k\tau} \\
&\quad \times \sum_{n=-\infty}^{\infty} J_n\left(\frac{\Delta\omega\delta\tau}{2}\csc\left(\frac{\pi}{f}\right)\right) e^{\pm in\pi\frac{2k+1}{f}} \\
&= e^{\mp i\Delta\omega\frac{\delta\tau}{2}} \sum_{n=-\infty}^{\infty} J_n\left(\frac{\Delta\omega\delta\tau}{2}\csc\left(\frac{\pi}{f}\right)\right) e^{\pm i\frac{n\pi}{f}} \\
&\quad \times \sum_{k=0}^{N-1} e^{\pm ik\left(\Delta\omega\tau + \frac{2n\pi}{f}\right)}
\end{aligned} \tag{A5}$$

where in deriving Eq. (A5), the Jacobi–Anger expansion, $e^{\pm iz\sin(\theta)} = \sum_{n=-\infty}^{\infty} J_n(z) e^{\pm in\theta}$ was used, where $J_n(z)$ is an nth order Bessel function. Using Eqs. (A1), (A5) reduces to:

$$\begin{aligned}
&e^{\mp i\Delta\omega\frac{\delta\tau}{2}} \sum_{n=-\infty}^{\infty} J_n\left(\frac{\Delta\omega\delta\tau}{2}\csc\left(\frac{\pi}{f}\right)\right) e^{\pm i\frac{n\pi}{f}} e^{\pm i\frac{(N-1)\left(\Delta\omega\tau + \frac{2n\pi}{f}\right)}{2}} \\
&\quad \times \frac{N\operatorname{sinc}\left[\frac{N\left(\Delta\omega\tau + \frac{2n\pi}{f}\right)}{2}\right]}{\operatorname{sinc}\left[\frac{\Delta\omega\tau + \frac{2n\pi}{f}}{2}\right]}
\end{aligned} \tag{A6}$$

References

[1] R.R. Ernst, J. Magn. Res. 3 (1970) 10.
[2] R. Kaiser, J. Magn. Res. 3 (1970) 28.
[3] R. Kaiser, J. Magn. Res. 15 (1974) 44.
[4] E. Bartholdi, A. Wokaun, R.R. Ernst, Chem. Phys. 18 (1976) 57.
[5] R.R. Ernst, J. Chem. Phys. 45 (1966) 3845.
[6] B. Blumich, Prog. Nucl. Magn. Res. 19 (1987) 331.
[7] M.H. Levitt, R. Freeman, J. Magn. Res. 43 (1981) 502.
[8] A.J. Shaka, J. Keeler, T. Frenkiel, R. Freeman, J. Magn. Res. 52 (1983) 335.
[9] U. Haeberlen, J.S. Waugh, Phys. Rev. 175 (1968) 453.
[10] L. Bosman, P.K. Madhu, S. Vega, E. Vinogradov, J. Magn. Res. 169 (2004) 39.
[11] G.S. Uhrig, Phys. Rev. Lett. 102 (2009) 120502.
[12] E.R. Jenista, A.M. Stokes, R.T. Branca, W.S. Warren, J. Chem. Phys. 131 (2009) 204510.
[13] H.Y. Carr, E.M. Purcell, Phys. Rev. 94 (1954) 630.
[14] R. Freeman, Chem. Rev. 91 (1991) 1397.
[15] B.L. Tomlinson, H.D.W. Hill, J. Chem. Phys. 59 (1973) 1775.
[16] R.J. Ordidge, Magn. Res. Med. 5 (1987) 93.
[17] M. Veshtort, R.G. Griffin, Chem. Phys. Chem. 5 (2005) 834.
[18] G. Bodenhausen, R. Freeman, G.A. Morris, J. Magn. Reson. 23 (1976) 171.
[19] G.A. Morris, R. Freeman, J. Magn. Reson. 29 (1978) 433.
[20] J. Kacynski, N.J.F. Dodd, B. Wood, J. Magn. Res. 100 (1992) 453.
[21] C. Roumestand, D. Canet, J. Magn. Res. 147 (2000) 331.
[22] J.J. Sakurai, Modern Quantum Mechanics, Addison-Wesley Publishing Co., New York, 1994.
[23] R.R. Ernst, G. Bodenhausen, A. Wokaun, Principles of Nuclear Magnetic Resonance in One and Two Dimensions, Oxford University Press, USA, New York, 1990.
[24] D. Canet, J. Brondeau, C. Roumestand, J. Magn. Res. Ser. A 117 (1995) 103.
[25] M. Shinnar, J.S. Leigh, J. Magn. Res. 75 (1987) 502.
[26] M. Shinnar, S. Eleff, H. Subramanian, J.S. Leigh, Magn. Res. Med. 12 (1989) 74.
[27] M. Shinnar, L. Bolinger, J.S. Leigh, Magn. Res. Med. 12 (1989) 88.
[28] C.R. Dybowski, R.W. Vaughan, Macromolecules 8 (1975) 50.
[29] M.M. Maricq, J. Chem. Phys. 86 (1987) 5647.
[30] M. Todica, R. Fechete, B. Blumich, J. Magn. Res. 164 (2003) 220.
[31] M. Todica, B. Blumich, Int. J. Mod. Phys. B 18 (2004) 1571.
[32] R.L. Kleinberg, J.A. Jackson, Concepts Magn. Reson. Part A 13 (2001) 340.
[33] S. Michaeli, D.J. Sorce, D. Idiyatullin, K. Ugurbil, M. Garwood, J. Magn. Res. 169 (2004) 293.
[34] H. Geen, R. Freeman, J. Magn. Res. 93 (1991) 93.
[35] L. Frydman, T. Scherf, A. Lupulescu, Proc. Nat. Acad. Sci 99 (2002) 15858.
[36] L. Frydman, A. Lupulescu, T. Scherf, J. Am. Chem. Soc. 125 (2003) 9204.
[37] R.P. Feynman, F.L. Vernon, R.W. Hellwarth, J. Appl. Phys. 28 (1957) 49.
[38] L. Viola, S. Lloyd, Phys. Rev. A 58 (1998) 2733.